Materials & Design 223 (2022) 111192

Contents lists available at ScienceDirect

Materials & Design

journal homepage: www.elsevier.com/locate/matdes

A generalizable and interpretable deep learning model to improve the prediction accuracy of strain fields in grid composites

Donggeun Park [a], Jiyoung Jung [a], Grace X. Gu [b], Seunghwa Ryu [a,*]

[a] Department of Mechanical Engineering, Korea Advanced Institute of Science and Technology (KAIST), 291 Daehak-ro, Yuseong-gu, Daejeon 34141, Republic of Korea
[b] Department of Mechanical Engineering, University of California, Berkeley, CA 94720, USA

HIGHLIGHTS

- Proposed multiscale kernel neural network (MNet) to predict the strain field of grid composite over vast design space.
- Demonstrated the excellent generalizability of predicting strain field of unseen volume fraction domain and unseen symmetric configurations compared to the state-of-the arts U-Net.
- Maintained superb predictive performance with less than one-third of dataset, and applied the MNet with the small input dimension to the larger system.
- Revealed the inference mechanism of black-box model (MNet) in predicting the vast design space.

GRAPHICAL ABSTRACT

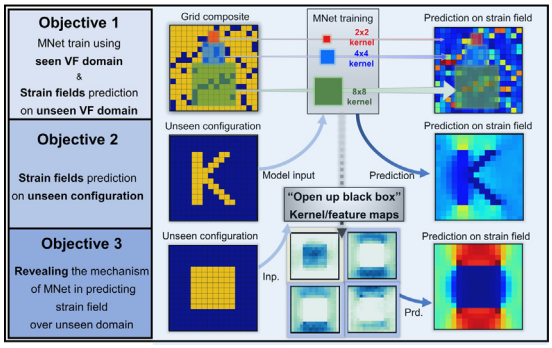

ARTICLE INFO

Article history:
Received 11 July 2022
Revised 20 September 2022
Accepted 21 September 2022
Available online 22 September 2022

Keywords:
Deep neural network
Interpretable deep learning
Composite design
Strain field
U-Net
Material design

ABSTRACT

Recently, the design of grid composites with superior mechanical properties has gained significant attention as a testbed for deep neural network (DNN)-based optimization methods. However, current designed DNN architectures are not specifically tailored for grid composites and thus show weak generalizability in exploring unseen configurations that stem away from the training datasets. Here, a multiscale kernel neural network (MNet) is proposed that can efficiently predict the strain field within a grid composite subject to an external loading. Predicting the strain field of a composite is especially important when it comes to understanding how the material will behave under loading. MNet enables accurate predictions of the strain field for completely new configurations in unseen domain, with a reduced mean absolute percentage error (MAPE) by 50% compared to a benchmark, U-Net as current state-of-the arts DNN architectures. In addition, results showed that MNet maintained superb performances with less than one-third of dataset, and can be applied to grid composites larger than the composite configurations used for the initial training. By investigating the inference mechanisms from the kernels of multiple sizes, our work revealed that the MNet can efficiently extract various spatial correlations from the material distribution.

© 2022 The Authors. Published by Elsevier Ltd. This is an open access article under the CC BY-NC-ND license (http://creativecommons.org/licenses/by-nc-nd/4.0/).

* Corresponding author.
E-mail address: ryush@kaist.ac.kr (S. Ryu).

https://doi.org/10.1016/j.matdes.2022.111192
0264-1275/© 2022 The Authors. Published by Elsevier Ltd.
This is an open access article under the CC BY-NC-ND license (http://creativecommons.org/licenses/by-nc-nd/4.0/).

1. Introduction

Developing composite materials with superior mechanical properties is key to solve the challenges in various applications in material science, medical engineering and automotive engineering [1–5]. Conventionally, particulate-reinforced or laminated composites with relatively simple configurations were widely used, which led to the development of analysis and design methods relavant to those configurations [6–8]. However, the advancement of multimaterial 3D printing methods opens a completely new design space for composite materials [9–11]. In order to fully exploit the advantage of multimaterial 3D printing, one needs to consider an astronomically large number of configurations. Hence, various optimization frameworks leveraging the superior inference of deep learning models have been proposed to handle such a large design space [12–15]. Furthermore, the two-dimensional grid composite design problems have served as a testbed for deep neural network (DNN)-based design methods paired with finite element method (FEM) [16–21]. FEM has been used for data generation for many deep learning based predictive modeling tasks, because FEM analyses match well with experimental results quantitatively in the elastic regime and qualitatively beyond the elastic regime [16]. Recently, the relationship between vast design parameters and objective functions in various engineering fields as well as in the material field has been investigated by directly learning through DNN methods [20,22,23].

However, there exist two major challenges in handling a grid composite design problem with deep learning, (i) large design space, and (ii) weak predictive power of a DNN in unseen domain. For example, a two-constituent composite with a 16x16 grid has a total 10^{77} distinct available combinations. Even if one generates one million different grid configurations for the training of a DNN, the fraction of training set in the design space is negligible (less than $1/10^{71}$ of all possible combinations). Still, the superior performance of DNN inference led to an efficient and accurate prediction of the properties for new grid configurations (located relatively close to the training set), when a convolutional neural network (CNN) architecture is adapted or an appropriate dimension reduction method is integrated.

However, in search for the optimal configuration far from the initial training set, relatively weak predictive power of a DNN in unseen domain limits the application of DNN-based optimization frameworks. For instance, the initial training set typically consists of random arrangements of two constituents, while the configuration with optimal stiffness or strength is likely to be a more ordered and symmetric structure [16,24]. As a solution, our previous study suggested a DNN-based optimization framework using active-learning to gradually expand the reliable prediction range of a DNN in search for the optimal configuration [24,25]. Moreover, if the configurations in the training set have a limited range of volume fraction ratio between two constituents, a DNN often does not accurately predict the properties of a grid composite with a very different ratio [24]. Furthermore, existing studies concerning the mechanical properties of grid composites only utilized publicly available DNN architectures so far that were not specifically developed for the grid composites. The weak generalization of a DNN in exploring unseen domain may not be overcome by just tuning the architecture of the neural network [24].

Predicting the strain field of a composite is especially important when it comes to understanding how the material will behave under loading. A new DNN architecture may have superior generalization performance if it can efficiently capture the correlation between the strain field and the configuration. Because of the mathematical similarity between elasticity and other physical phenomena (thermal conductivity, piezoelectricity, thermoelectricity, and etc) [26], such an architecture can be beneficial for the grid composite design problems concerning various physical properties. U-Net, which was originally developed for biomedical image segmentation, has shown a superior performance in predicting local fields over the composite problems because U-Net [18,27] has an architecture that efficiently compresses and recovers the spatial information between constituents compared to conventional DNNs [16] which cause information loss during the convolution operation. However, U-Net architecture has limitations in learning the grid composite properties. For example, the architecture drops the information generated in layer of neural network. In addition, the fixed kernel size has been used to capture the strain field despite the importance of diverse information obtainable from various convolution kernel sizes [28,29]. As a result, the U-Net does not provide satisfactory predictive power to predict the configuration in unseen domain [23]. Although the U-Net using data augmentation and transfer learning is a solution of predicting local fields over the unseen domain and large system, these still bring out generating extra simulations/experiments and training an extra deep learning model.

Therefore, in this study, a novel multiscale kernel neural network architecture, named as MNet, is proposed to tackle these challenges, as shown in the schematic in Fig. 1. MNet is a single-shot training neural network architecture for grid composite designing tasks without relying on iterative active-learning and data augmentation. While the existing DNN models (U-Net) have employed a single-scale kernels, the MNet employs a multi-scale kernel method with reduced feature maps to efficiently extract the correlation between input (configuration) and output (strain fields). The extension of kernel size obtainable from various effective convolution kernel sizes can compensate the information loss caused by reduction in numbers of feature maps [28,29]. Also, the extracted feature maps are fused and complemented each other. In addition, MNet employs a feature reuse method to minimize the information loss during the neural network operation (explained as follow "method" chapter in detail). The superior performance of MNet is demonstrated in terms of three aspects; generalization performance (prediction accuracy over the configurations outside the training set), training efficiency (prediction error for a given dataset size), and applicability (prediction to larger grid composites using MNet trained for small grid composites without retraining). Finally, we delve into the mechanism of MNet behind the superior generalization performance over the configurations within the unseen design space. Hyperparameters of MNet are tuned by manually experimenting with different sets of hyperparameters using trial and error methods. The training results from the U-Net architecture, which have shown the best performance over the grid composite problem so far, are used as a benchmark. In this work, we focus only on the local elastic strain distribution over the linear response regime; an interesting future work direction is applying to the plastic regime.

2. Method

2.1. Data collection for showing deep learning model's generalizability.

In general, a deep learning model is developed using data sets which are divided into training and test sets. The training and test sets are used to develop deep learning model and to evaluate the predictive performance of the model, respectively. Input of the each training/test set is a 2D matrix composed of 0 and 1 representing two constituent materials in the configuration, and the output is the normal strain component along x-direction (ε_{xx}) at each block, respectively (Fig. 2a).

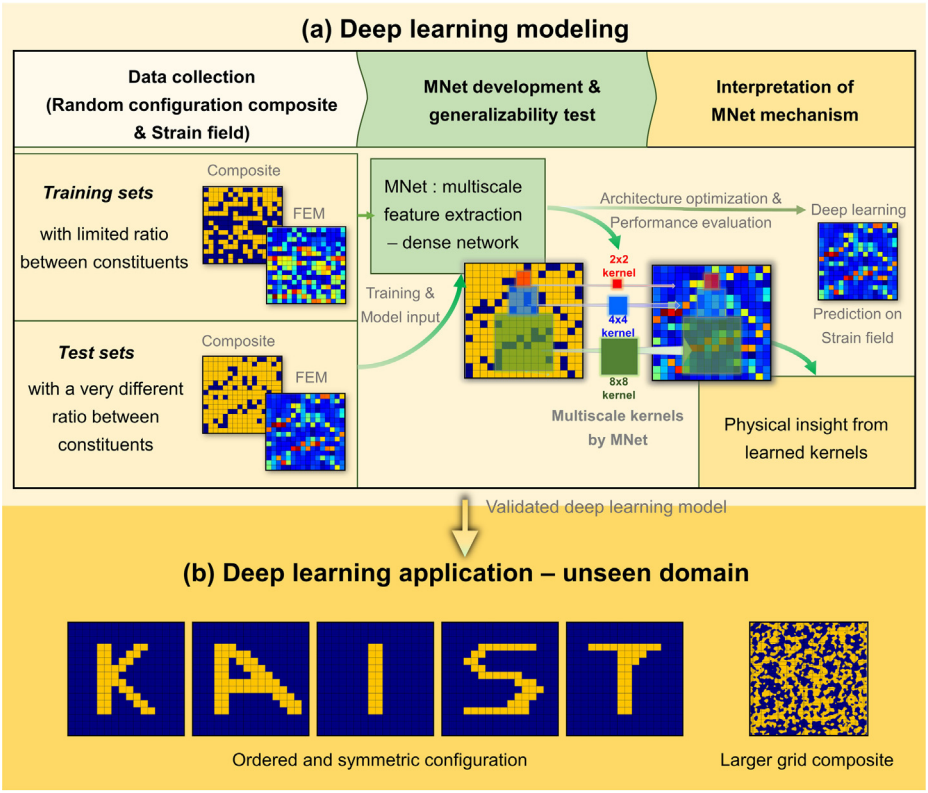

Fig. 1. Schematic of a novel deep learning method (MNet) to predict strain fields from configurations of composites within unseen design space. (a) The deep learning model is trained from random configurations having 3 discrete volume fractions (VF) of 30%, 50%, and 70%. To investigate the generalizability of deep learning model, the trained model is evaluated using test set which has the extensive VF space (1–99%) compared to training set. The model mechanism are investigated via the interpretation of kernels/feature maps at final layer to validate the superb predictive performance for the unseen design space. (b) The trained model is investigated to the further challenge problem of unseen domain (ordered and symmetric configurations) and prediction on strain field of large grid composites (256 × 256) using MNet trained with small grid composites (16 × 16).

To ensure the generalizability of deep learning model over the unseen domain, the test set should include the vast design space of a grid composite in terms of randomness in their distribution and VF of stiff material, as shown in Fig. 2b. We then train the MNet and benchmark model with the initial training set from random configurations having 3 discrete VFs of 30, 50, and 70% (Fig. 2c). To make a reasonable comparison between the benchmark model and the MNet model, we examine the hyperparameters of the benchmark model. The learning hyperparameters of MNet are the same as the benchmark, but employing the novel architecture modeling methods. See the details of hyperparameter optimization in Figs. S1 and S2. Two different test sets are prepared; "*test set i*" consists of random configurations having VFs ranging from 1% to 99% (Fig. 2d), and "*test set ii*" contains ordered configurations (Fig. 2e). One can test the generalization performance of the MNet in terms of unseen VF range or unseen configuration symmetry.

2.2. Data sets generation using finite element method (FEM)

Grid composites can have a variety of configurations depending on their arrangement. A microscopic image can be considered a grid composite and converted to a binary image for FEM [30,31]. FEM with rational accuracy is an efficient alternative to time-consuming and expensive experiments. Therefore, we developed the deep learning model based on FEM data to explore the configuration-strain field relation.

Once the data sets representing the aforementioned seen/unseen design space are generated, the corresponding 2-D strain fields are obtained from SfePy package (simple finite elements in Python), which is a software for solving various kinds of problems described by patial diffenerential equation by FEM method [32]. The FEM simulation was performed in the elastic regime. Two elastic contrast ratio are tested to show the predictive performance of deep learning model. Young's modulus of soft and stiff phases for two materials were 10/120 GPa and 100/120 GPa, respectively, and Poisson's ratios for both phases were 0.3. The periodic boundary conditions (PBC) are applied for FEM, which enables reasonable prediction for macro behavior from the unit cell [33,34].

For analysis of 16x16 grid composite system, 256 CPS8 elements are used, and strain values are averaged for each element. For the FEM, macro strain of 2% in x-direction (ε_{11}) is applied to the composites and the rest of macro strain (ε_{ij}, where i, j = 1,2) are set to zero. Since multi-axial deformation can be considered by the superposition of uniaxial deformation, there is no need to create a deep learning model for multi-axial deformation. Therefore, we simply apply the macro strain in x-direction (ε_{11}) for training deep learning model.

2.3. Deep learning neural network (multi-scale kernels network, MNet)

MNet has a novel convolution method and network architecture, which efficiently extracts the relation between the composite configuration and corresponding strain fields. The detail of MNet, named as "Multi-scale kernels network", is as follows;

(i) MNet first takes the 2D grid composite (16 by 16 elements) as input. The encoder section of MNet on the left of Fig. 3a extracts the spatial-interactive information between the

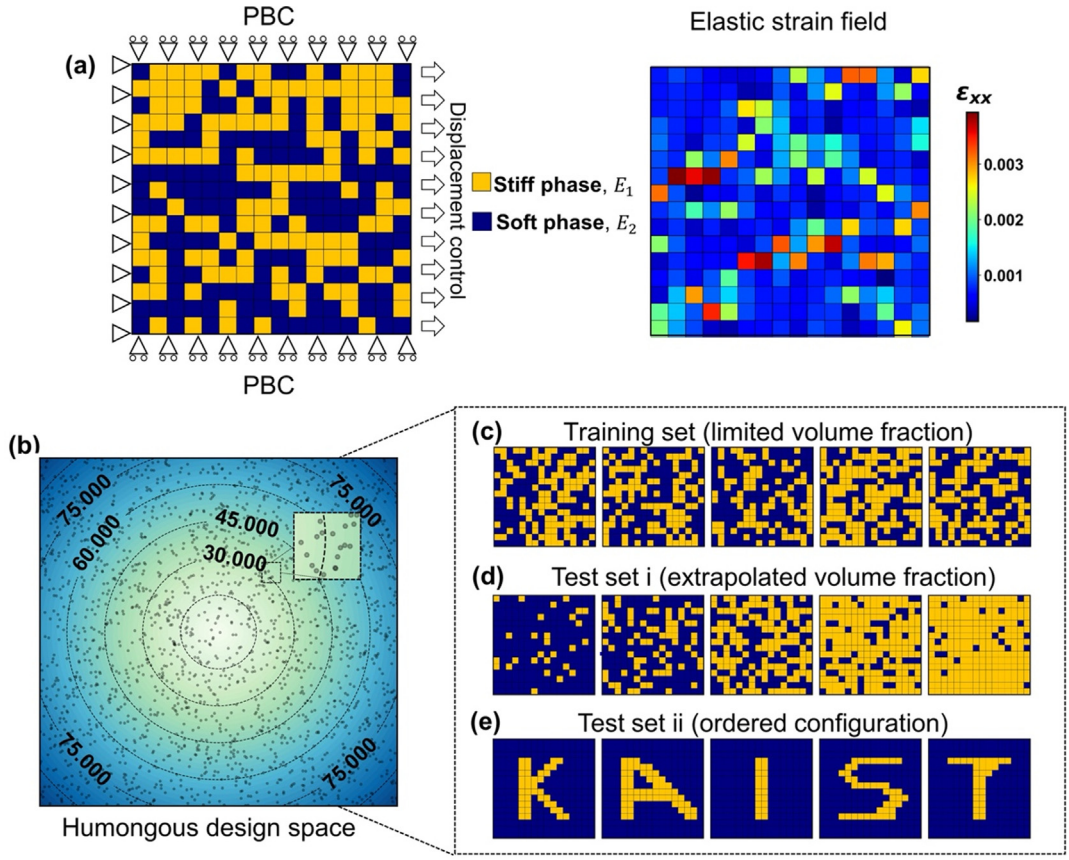

Fig. 2. Data set generation to reasonably represent the design space problem. (a) Schematic of 16 × 16 grid composite composed of stiff and soft materials, the applied boundary conditions and corresponding strain field by FEM and corresponding strain field by FEM. (b) An example of design space due to an astronomical combination of constituents. The dots represent configurations ditrtibuted by numerous two-constituents. (c) Training set with random configuration within limited volume fraction (30%, 50% and 70% VFs). (d) Test set i with random configuration within the completely different ratio of constituents from the training set (1–99% VFs). (e) Test set ii with ordered and symmetric configurations.

constituents, which correlate with the strain field. The convolution operation is carried out to extract the spatial information of constituents by simultaneously moving multi-dimensional kernels (2 × 2, 4 × 4 and 8 × 8 size) as shown Fig. 3b.

(ii) The kernel size of the convolution is related to the local receptive field, which extracts the various spatial relationship between the composite constituents depending on dimension of kernels. More specifically, the correlations between adjacent constituents are extracted using a low-level kernel, and effects between distant constituents are captured using a high-level kernel (Fig. 3b). The composite constituents-strain field relation extracted by multiple kernels is verified in the results section.

(iii) However, since the multi-scale kernels method causes a problem in that the number of feature maps increases, we divide the number of convolutional feature maps by the number of multi-kernels (Fig. 3c). Because three-scale kernels are used in this study, N feature maps were evenly divided to N/3 feature maps to prevent increase of trainable parameters of deep learning model (when N is not divisible by 3, we round down N/3).

(iv) Next, the convolution operation is calculated with same-padding to preserve the spatial dimension by the following equation.

$$S_{ij}^{(k)} = \sum_{a=\lceil -\frac{m}{2} \rceil}^{\lceil \frac{m}{2} \rceil} \sum_{b=\lceil \frac{n}{2} \rceil}^{\lceil \frac{n}{2} \rceil} I_{i-a,j-b} K_{\frac{m}{2}+a,\frac{n}{2}+b} \quad (1)$$

where $S_{ij}^{(k)}, I_{i-a,j-b}$ and $K_{\frac{m}{2}+a,\frac{n}{2}+b}$ are the calculated feature map, the input matrix and kernels, respectively. m and n is slide size. The results of multi-scale kernels transfer to batch normalization (BN) layer. It accelerates the training process by controlling a parameter scale [35]. The BN results have the non-linearity characteristic by converting an activation function (ReLu). The convoluted feature maps are fused through "feature fusion layers" because the multi-kernel results contain meaningful information for configuration-strain field relations in the various viewpoints (Fig. 3c). The feature fusion layer is represented as the following equation:

$$S_{lm} = S_{ij}^{(1)} \oplus S_{ij}^{(2)} \oplus S_{ij}^{(3)} \quad (2)$$

Where $S_{lm}, S_{ij}^{(1)}, S_{ij}^{(2)}$ and $S_{ij}^{(3)}$ are the fused feature maps, feature maps by first kernel, feature maps by second kernel and feature maps by third kernel, respectively.

(v) Then, the merged feature maps are used as input in next layer. Here, each of feature maps calculated from all previous sub-layers are concatenated as next inputs as shown in Fig. 3c. Reusing all information from previously calculated feature can minimize information loss during convolution process. In addition, the feature reuse method contributed to the effect of fast convergence of the learning error by minimizing overfitting and reducing effects such as gradient exploding [36]. These learning effects are represented in Fig. S1. Next, the 1x1 convolution, which is a pointwise method [37], reduces the learning weight and maintains meaningful information, as shown in Fig. 3d. The down-

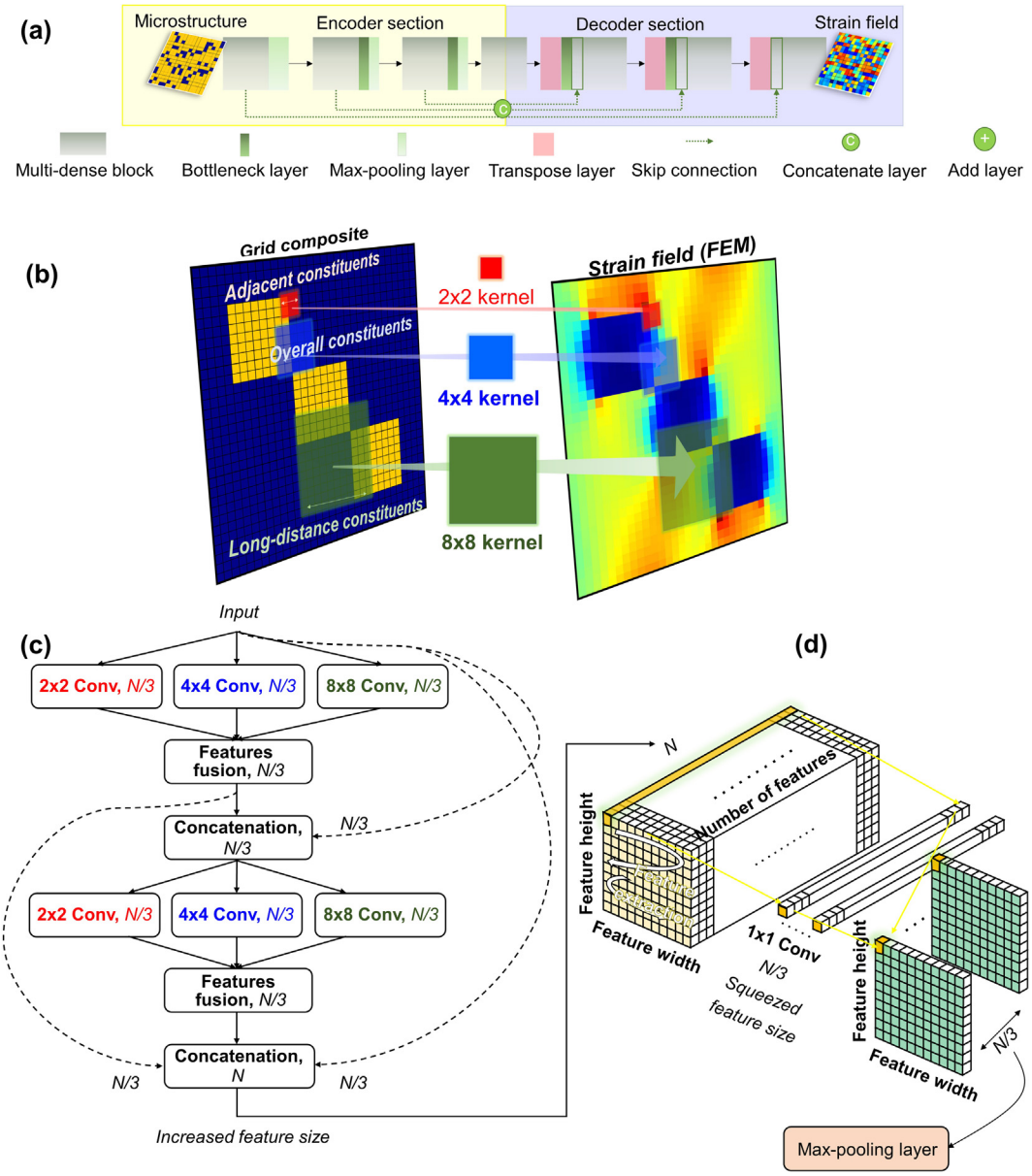

Fig. 3. Multiscale kernel neural network (MNet). (a) The architecture is based on U-Net backbone. We modified the general U-Net backbone using our advanced method. (b) Multi-feature extraction method with multi-dimensional kernels. (c) Multi-dense block with multi-feature extraction method, dense layer method and (d) pointwise method (bottleneck layer) to squeeze the increased feature maps. The final feature maps are finally connected to max-pooling layer.

sampling layer (max-pooling, m × m size) leads to the reduction of the feature map's dimension preserving the important information. It extends the receptive field size which increases the robustness for the distant composite constituents and decreases the computation load.

(vi) The multi-kernels dense block in encoder section is repeated two times to extract the interaction between composite constituents. Next, we use the decoder section using the transpose convolution operation on right of Fig. 3a. The decoder section increases the dimension of final feature maps reduced in encode section by the FEM spatial dimension and predicts the FEM results by optimizing the CNN weight. The transposed convolution operation is used to restore the squeezed feature maps by moving multiple learned CNN filters (3 × 3 size, 2 stride).

(vii) Then, the transposed convolution feature maps are linked with the corresponding feature maps in each of last layers in encoder section (e.g. concatenate layer) to complement the spatial-interactive information between the constituents (Fig. 3a). Then, the multi-scale feature maps connected from encoder section and the transposed feature maps are concatenated and transferred to the multi-dense block without down-sampling layer. This process is repeated to restore the output dimension (FEM results). We use the linear activation function in the final output layer for the regression problem.

Here, the benchmark algorithm (U-Net) only uses the general single-kernel without feature reuse. Although MNet and U-Net have the same number of feature maps, MNet has 4,796,494 learning weights. U-Net has 12,724,737 weights. That is, the MNet can be effectively trained using only 37% of the benchmark weights.

The learning weights between input and output are repeatedly optimized by with the gradient of the loss function backpropagation algorithm. MNet is updated by backpropagation of Adam optimizer [38]. We use the mean square error as loss function. In this

study, MNet and U-Net is implemented using Keras with TensorFlow backend.

3. Results

3.1. Deep learning model's generalizability test for extensive design space: Unseen volume fraction range.

Fig. 4 shows the results predicted by the MNet and the benchmark U-Net over the "*test set i*" containing 1,980 random configurations with VFs ranging from 1% to 99%. We test the two different ratios of elastic constants to show generalizability over different constituent materials. The two models are sufficiently converged after 5 training iterations, indicating that they can be reasonably compared with each other (see the details of repeatability test of deep learning models in Fig. S3). In the interpolation range within 30 to 70% VF, MNet outperforms the benchmark notably. Still, the performance of the U-Net turns out to be reasonably good within the range. However, in the unseen VF domain outside the training set, the performance of the U-Net starts to degrade significantly especially in the VF ranges located farther, as depicted in the R^2 (Fig. 4a,c) and mean absolute percentage error (Fig. 4b,d). On the contrary, the performance of MNet persists beyond the VF range of the training set, and a notable drop in the prediction accuracy is found only near to the limiting cases of 1 or 99 % VFs. In addition, the superb predictive performance of MNet is maintained regardless of change in elasticity ratios.

Additionally, in Fig. 5, we visualize the error distribution, scatter, and heatmap for the strain fields where predictions of the deep learning models are compared to FEM results for randomly selected two configurations in the "*test set i*" in the interpolation (VF = 52 %, Fig. 5a–c) and extrapolation (VF = 10%, Fig. 5d–f) ranges. At a first glance, both MNet and benchmark seem to successfully predict the local strain distribution, because strain field predictions from both looks similar to that of FEM as shown in Fig. 5c and f. However, the error distribution histograms (Fig. 5a and d) and MAPE heat maps (Fig. 5c and f) more clearly visualize the superior performance of the MNet over the benchmark. MNet shows narrow error distribution with small errors for both interpolation and extrapolation tasks, while the benchmark leads to relatively wider error distribution with relatively higher errors for extrapolation tasks. Our results imply that the MNet is able to learn the configuration-strain field relationship over a wide VF range, even if it was trained with a training set with limited VF ranges. In addition, because of the superior inference of MNet, MNet requires only less-than one-third of training dataset to achieve the same level of error compared to the benchmark (see the details of results of deep learning training efficiency test in Fig. S4).

3.2. Deep learning model's generalizability test for unseen domain: Ordered configuration.

Next, we test the generalization performance of the MNet over a more challenging interference task of predicting the strain field of ordered configurations. In pattern or shape optimization tasks via

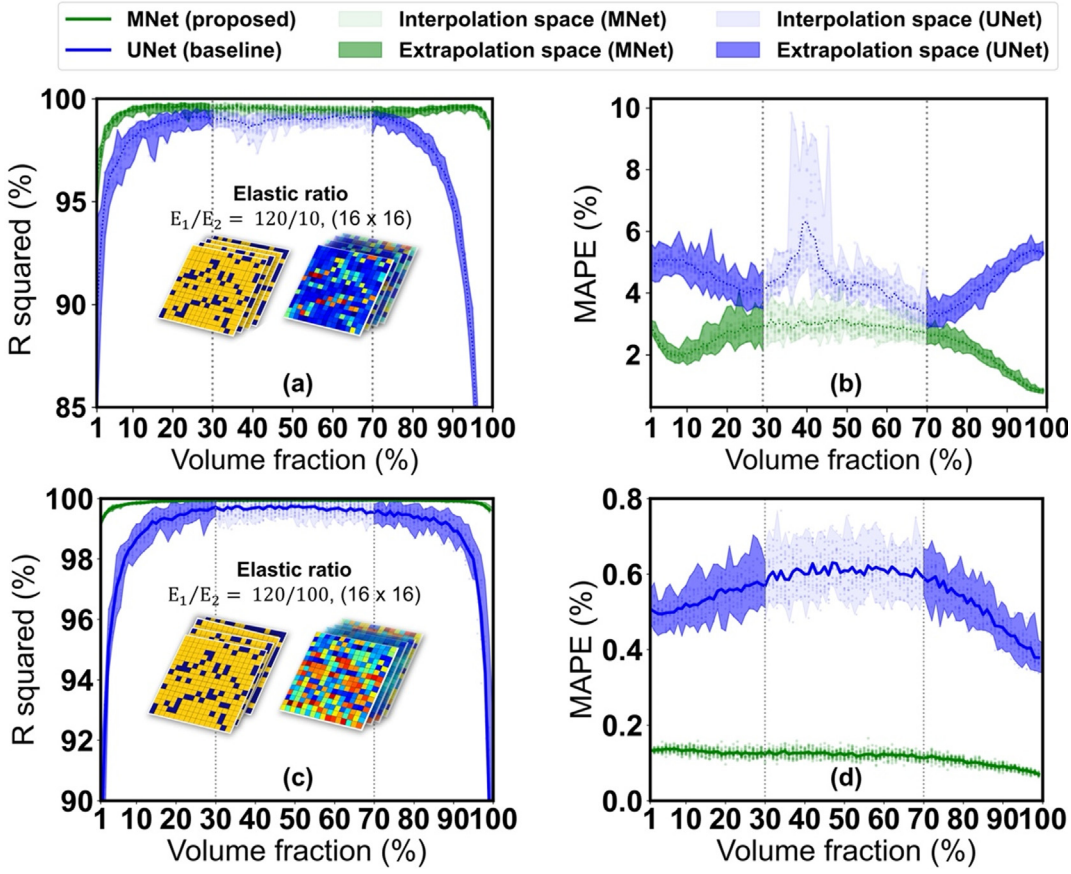

Fig. 4. Results of model generalizability test over extensive design space for two elastic constrast ratio (E_1/E_2 = 120/10 and 120/100). Deep learning models (MNet and baseline) are evaluated using the aforementioned *test set i*. Performance of MNet is compared with that of U-Net in terms of (a, c) R^2 and (b, d) MAPE, respectively. MNet shows the superb generalizability of predicting strain fields with seen and unseen volume fraction compared to the baseline. However, baseline degrades the predictive performance in unseen VF domain (VF 1–30% and 70–99%).

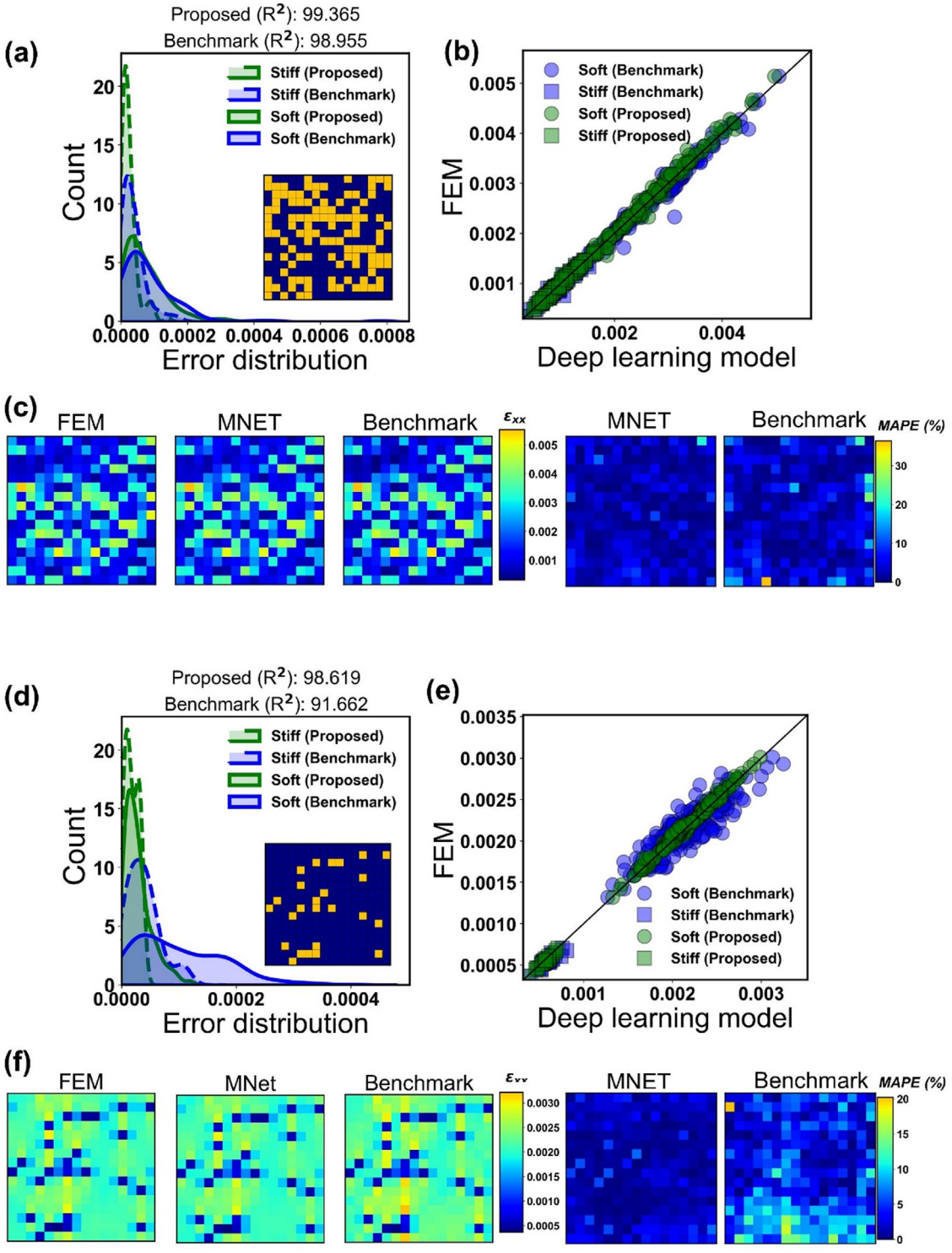

Fig. 5. Analysis on the strain fields predicted by deep learning models (MNet, baseline) and FEM. Composites are randomly selected in interpolation (VF 52 %) and extrapolation (VF 10%). Two configuration in interpolation and extraploration are shown in a, d, respectively. Absolute error histogram of strain fields by the deep learning models and FEM are illustrated in a, d. The error histograms are calculated separately for stiff and soft phases. Also, their strain fields of all elements by deep learning models are compared to the FEM results (ground truth) using scatter plot in b, e. The variation of baseline are increasesd for configuration within unseen volume fraction. However, MNet shows superb generalizability which is similar ideal fitting line. Heat maps about the composite within interpolation and extrapolation are shown by FEM, deep learning models in c, f. Baseline shows non-uniform MAPE heatmap compared to MNet.

deep learning, DNN trained over a training set consisting of random configurations has weak predictive power over the optimal configuration (typically, ordered and symmetric configuration), limiting the applicability of DNN-based inverse design method [18,20]. To overcome the problem, our previous study proposed a neural network-based forward design framework in which the reliable prediction range gradually expands via active learning and data augmentation [24]. Hence, in the "*test set ii*", we construct

multiple ordered configurations motivated by the KAIST logo to test the generalization performance of the MNet trained over random configurations, as depicted in Fig. 6.

The strain fields predicted from MNet matches very well with those obtained from FEM, i.e. the ground truth. On the contrary, the strain fields predicted from the benchmark deviate from the ground truth for the unseen ordered configurations. Here, the MNet reduces the MAPE for the strain distribution by 55%, when compared with benchmark results. The generalization performance over two test sets implies that the MNet may serve as an efficient single-shot training surrogate model for grid composite designing tasks without relying on iterative active-learning based optimization approaches.

3.3. Application of deep learning model to predict large composite

Having tested the generalization performance of the MNet over unseen domain involving grid composites of the same size, we test its ability to predict the strain field of larger grid composites. It is desirable to have such a capability because the FEM analyses of larger grid composites require expensive computational cost and longer computation time. Also, if it becomes feasible, we do not need to train an extra deep learning model when designing grid composites whose size is larger than the grid composites used in the original training set.

In the literature, a divide and conquer (DaC) algorithm has been suggested to apply the deep learning model with the small input dimension to the larger system [39,40] and utilized to date, of which schematic is shown in Fig. 7a. The general DaC algorithm breaks down a large composite into many sub-composite parts, until their dimensions become identical to the input dimensions of the deep learning model trained with a small composite system. The sub-composites are fed into to the model, and the prediction results for strain fields of sub-composites are rearranged by the large composite dimension as shown Fig. 7a. However, the general DaC scheme may cause informative loss because the spatial correlation is not shared among the divided small composites (Fig. 7b). This may lead to a decrease in the prediction accuracy of the strain field of large composite systems.

Therefore, a novel overlapping DaC method is proposed to minimize the information loss. The overlapping DaC divides the large composite by mimicking the CNN stride method that controls how filter convolves over the input image. More specifically, our method first splits the large composite into small domains, as well as overlapping domains to include the boundary region between them as shown Fig. 7c. Then, all divided composites including the rest of the red and green box in Fig. 7c are fed into the model. All predicted strain fields are rearranged using only the 8x8 region from the center, excluding region where information is likely to be lost at the boundary. We compare the strain error distributions of the 256x256 size composites predicted by the general DaC and our novel overlapping DaC system, as shown in Fig. 7d. To compare the two methods, we identically use a MNet trained with a 16x16 grid, and use a large composite and the strain fields of FEM in Fig. 7a.

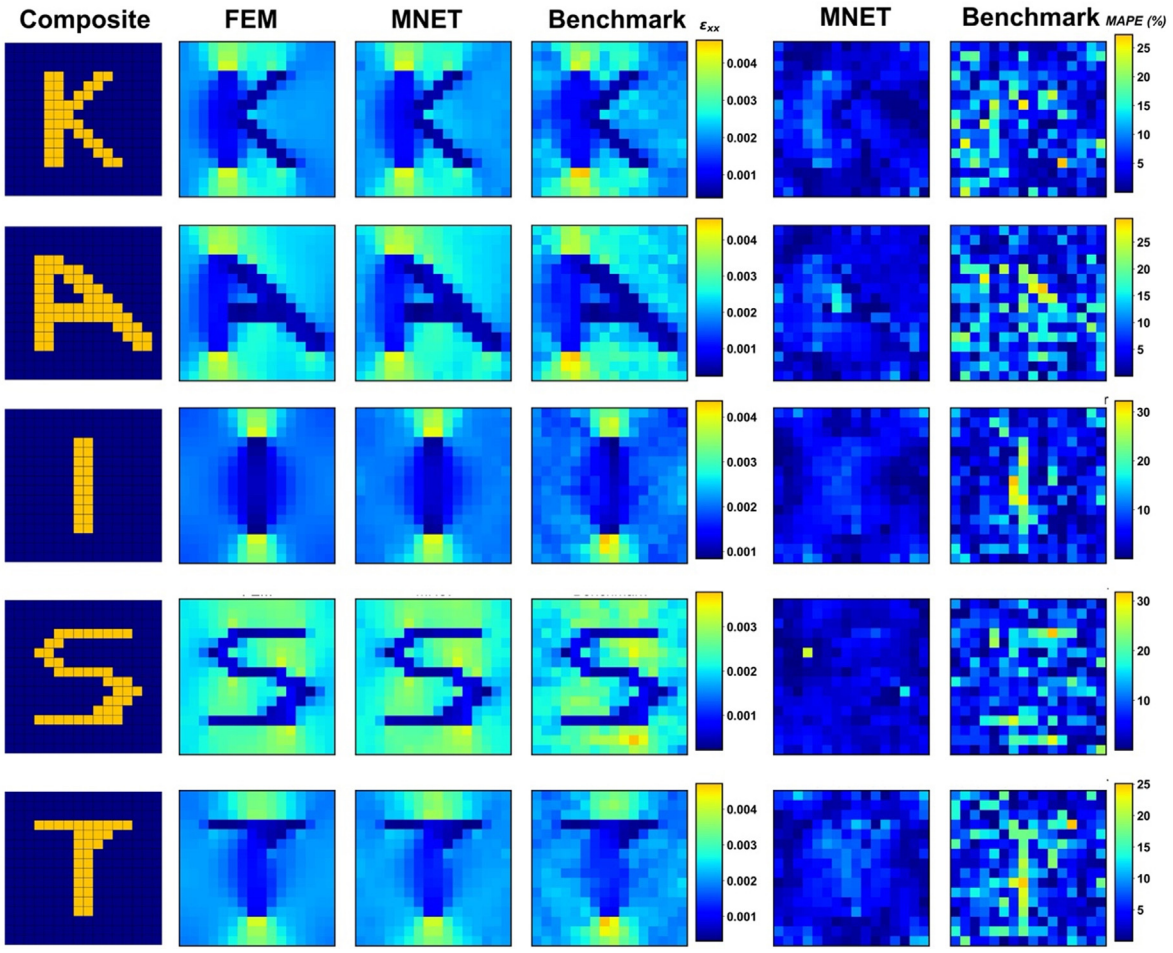

Fig. 6. Further complex model generalizability test results using ordered configuration far away from the training configuration. Generalizability test are performed using totally disparate geometric pattern from the training set. The evaluation is conducted in terms of MAPE.

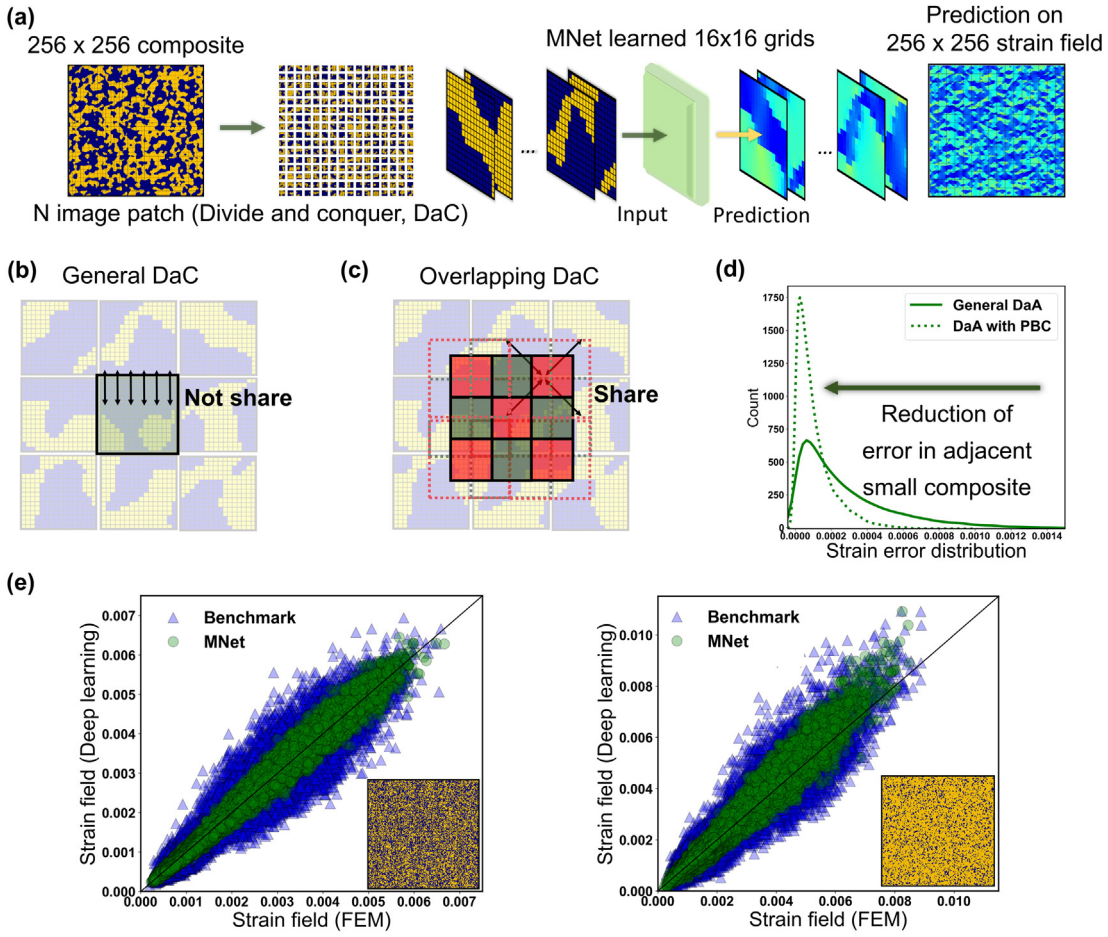

Fig. 7. (a) Deep learning model application to predict the large composite (256x256) using 16x16 MNet and custom-divide-and-conquer (DaC) method. (b) General DaC method and (c) Overlapping DaC method (d) Comparison of the general DaC with the overlapping DaC for the large composite. (e) Prediction results of the two large composites (VF = 52% and 82%, respectively) by MNet and U-Net with overlapping DaC.

Compared to the general DaC, the overlapping DaC efficienctly increases the prediction accuracy for strain fields of large composite because the spatial correlation information is shared via the overlapping patches.

Additionally, the overlapping DaC is applied to the the benchmark model and the MNet model to test their ability to predict the strain field of larger grid composites, as shown in Fig. 7e. We use two large composites with the random configurations (VF = 52% and 82%). Benchmark model with the low generalizability have significant error variations in predicting the strain fields of the two large composites compared to MNet with high generalizability for an unseen domain. The applicability of MNet with the overlapping DaC implies that the combined methods may serve as an efficient approach that does not require re-training a deep learning model when designing larger grid composites.

3.4. Interpretation of inference mechanism of the learned MNet and benchmark model

Next, the mechanism behind the superior generalization performance on unseen design space is analyzed. Kernels/feature maps at the last block of learnt deep learning model have the most highly task-relevant features and have provided the learning mechanism of DNN models applied to various science and engineering disciplines [41-43]. Based on the methods, we investigate the characteristics of multi-kernels and corresponding feature maps of MNet and benchmark model by visualizing the inference process of unseen configuration at the final block as shown Fig. 8.

A single configuration containing square-shape stiff phase embedded in a soft phase is fed into MNet and benchmark trained with the random configurations (Fig. 8a). To facilitate the mechanism interpretation, four kernels in MNet and benchmark are randomly selected and analyzed. The multiple kernels of MNet efficiently extract the significant strain information between the constituents depending on the receptive field of kernels (see the details of results of kernels/feature maps at final layer of the trained models in Fig. S5e-g). These extracted information are all relevant in predicting the strain field of unseen configurations. Therefore, one can conclude that all feature maps complement each other through the fusion layer and 1d-pointwise convolution (a detailed explanation on the architecture is provided in the "Method" section). The complemented feature maps are illustrated in Fig. 8b. These feature maps of MNet extract the explainable strain information compared to the results of strain fields by FEM (Fig. 8d). The comprehensible feature maps are passed through the final activation function (Fig. 8c) and the resulting prediction turns out to be very similar to the ground truth (Fig. 8d).

It is of note that the learnt kernels of benchmark model are irregular compared to the kernels of MNet (Fig. S5). These benchmark kernels extract the corresponding non-uniform strain information of unseen configuration as shown Fig. 8e. Some feature maps do not reflect the ordered and symmetric strain distribution and look rather irregular. These irregular feature maps cause the

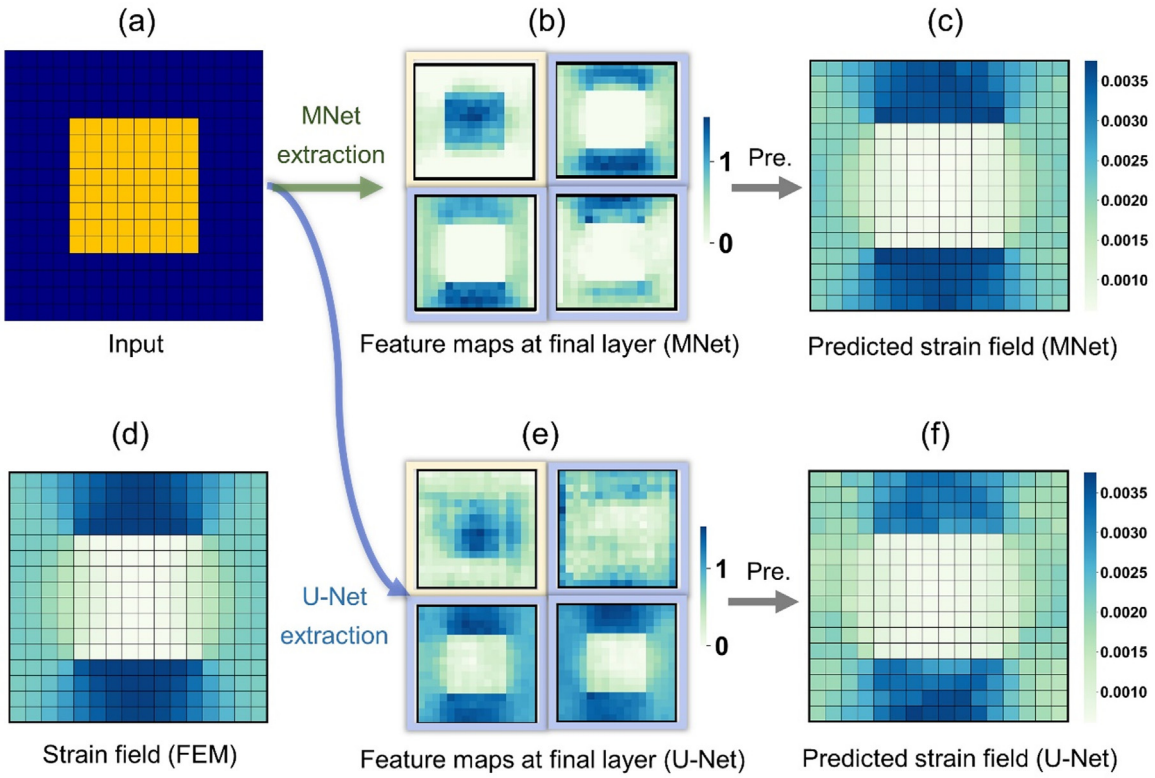

Fig. 8. Interpretation on kernels/feature maps at final block through visualizing inference process of unseen configuration to reveal inference mechanism of MNet algorithm with superb generalizability. (a) Configuration that is completely different from the training space. (b) Feature maps of MNet through multi-feature extraction method, fusion layer and pointwise method at final layer. The orange box and blue box represents the strain field information of stiff phase and the strain field information of soft phase, respectively. These can be explained by comparing with results of FEM. (c) Results of strain field predicted by MNet. (d) Strain field distribution by FEM simulation. (e) Feature maps through single kernel by benchmark (U-Net). (f) Results of strain field predicted from benchmark (U-Net). The benchmark model extract the non-uniform strain information, which bring outs the degradation of generalizability for predicting strain field of unseen configuration.

degradation of generalizability of predicting unseen configurations as shown Fig. 8f. In addition, even when a configuration containing a larger square-shaped rigid phase included in the soft phase is fed, MNet outperforms the benchmark model results with various single kernel size and generalizes the results of interpretation of deep learming model mechanism (Fig. S6). In other words, multiple-kernel method combining feature reuse and pointwise method is key to predict the configuration-strain field relation the unseen design space.

4. Discussion

In this study, we propose a novel DNN architecture called MNet to predict the strain field of grid composite within large and unseen design space in the elastic regime. We verify the performance MNet in terms of three aspects: generalization performance, training efficiency, and interpretability. The MNet trained with random 16x16 configurations shows excellent predictive performance even for unseen configurations. Although MNet is trained with random configurations with limited VFs (30%, 50%, and 70%), it successfully predicts strain field for a wide range of VF as well as ordered symmetric configurations. Although iterative learning frameworks based on active learning and data augmentation may provide solutions to the problem of weak-predictive performance in unseen configurations [24,25], MNet can be an efficient alternative for vast design space problem as a single-shot training model without data-augmentation and re-training. In addition, we show MNet trained with small grid composite (16×16) can predict strain field of large grid composites (256×256). We propose the so-called overlapping DaC method inspired by the convolution stride method to minimize the information loss occurring in the existing DaC method. The MNet combined with the efficient overlapping DaC outperforms the U-Net with overlapping DaC to predict the large composite system.

The inference process of multiple-kernls/feature maps at the final block is investigated to understand the generalizability performance of MNet over the unseen design space. In the prediction task on unseen domain (order and symmetric configuration), the MNet can extract meaningful features concerning the correlation between the configuration and the strain field. The feature maps containing strain field information complement each other, enabling the clear prediction of strain field for the unseen configurations. Opening the black box model allows domain experts in various engineering disciplines to provide insight into deep learning models. It is envisioned that MNet can be readily applied to a wide range of design problems with image-based input data in a variety of science and engineering disciplines.

5. Conclusion

In conclusion, we proposed multiscale kernel neural network (MNet) that accurately predict the strain field of composites far away from the VF domain of training dataset. Moreover, the MNet can predict strain fields for the symmetric and ordered configurations. It is of note that the benchmark (UNet) as the existing state-of-the-arts algorithm significantly degraded in predicting the unseen domain. MNet reduced mean absolute percentage error (MAPE) by 50% compared to a benchmark architecture (UNet). MNet maintained superb performances with less than one-third of dataset, and can be applied to grid composites larger than the

composite configurations used for the initial training. Furthermore, we revealed that the MNet efficiently extracted various meaning spatial correlations (feature maps) from the spatial distribution of constituents. Here, the benchmark generated irregular feature maps that cause the degradation of generalizability of predicting unseen configurations. In order to further explore materials with superior properties from deep learning model, it is necessary to extend deep learning capabilities beyond the elastic regime. We plan to apply the network architecture proposed in this study to tackle more complex material behaviors in a future study.

6. Data availability

The data obtained in this study are available from the authors upon reasonable request.

Declaration of Competing Interest

The authors declare that they have no known competing financial interests or personal relationships that could have appeared to influence the work reported in this paper.

Acknowledgements

This research was supported by National Research Foundation of Korea (NRF) (Fund Number: 2022R1A2B5B02002365), KAIST Global Singularity Research Program for 2022 (Fund Number: 1711100689), KAIST UP Program (Fund Number: N10220003), the Office of Naval Research (Fund Number: N00014-21-1-2604), and National Science Foundation (Fund Number: DMREF-2119276).

Appendix A. Supplementary material

Supplementary data to this article can be found online at https://doi.org/10.1016/j.matdes.2022.111192.

References

[1] K.I. Jang, H.U. Chung, S. Xu, C.H. Lee, H. Luan, J. Jeong, H. Cheng, G.T. Kim, S.Y. Han, J.W. Lee, J. Kim, M. Cho, F. Miao, Y. Yang, H.N. Jung, M. Flavin, H. Liu, G.W. Kong, K.J. Yu, S. Il Rhee, J. Chung, B. Kim, J.W. Kwak, M.H. Yun, J.Y. Kim, Y.M. Song, U. Paik, Y. Zhang, Y. Huang, J.A. Rogers, Soft network composite materials with deterministic and bio-inspired designs, Nat. Commun. 6 (2015) 1–11, https://doi.org/10.1038/ncomms7566.

[2] L.K. Grunenfelder, N. Suksangpanya, C. Salinas, G. Milliron, N. Yaraghi, S. Herrera, K. Evans-Lutterodt, S.R. Nutt, P. Zavattieri, D. Kisailus, Bio-inspired impact-resistant composites, Acta Biomat. 10 (9) (2014) 3997–4008.

[3] J.J. Martin, B.E. Fiore, R.M. Erb, Designing bioinspired composite reinforcement architectures via 3D magnetic printing, Nat. Commun. 6 (2015) 1–7, https://doi.org/10.1038/ncomms9641.

[4] F. Ahmad, H.S. Choi, M.K. Park, A review: Natural fiber composites selection in view of mechanical, light weight, and economic properties, Macromol. Mater. Eng. 300 (2015) 10–24, https://doi.org/10.1002/mame.201400089.

[5] M. Zhang, N. Zhao, Q. Yu, D. Ren, F. Berto, Z. Zhang, Z. Liu, R. Qu, J. Zhang, S. Li, R. O. Ritchie, On the damage tolerance of 3-D printed Mg-Ti interpenetrating-phase composites with bioinspired, Nat. Commun. 13 (2022) 1–13, https://doi.org/10.1038/s41467-022-30873-9.

[6] J. Jung, S. Lee, B. Ryu, S. Ryu, Investigation of effective thermoelectric properties of composite with interfacial resistance using micromechanics-based homogenisation, Int. J. Heat Mass Transf. 144 (2019) 118620, https://doi.org/10.1016/j.ijheatmasstransfer.2019.118620.

[7] J. Jung, S.H. Jeong, K. Hjort, S. Ryu, Investigation of thermal conductivity for liquid metal composites using the micromechanics-based mean-field homogenization theory, Soft Matter. 16 (2020) 5840–5847, https://doi.org/10.1039/d0sm00279h.

[8] Y. Kim, J. Jung, S. Lee, I. Doghri, S. Ryu, Adaptive affine homogenization method for Visco-hyperelastic composites with imperfect interface, Appl. Math. Model. 107 (2022) 72–84, https://doi.org/10.1016/j.apm.2022.02.007.

[9] M.A. Skylar-Scott, J. Mueller, C.W. Visser, J.A. Lewis, Voxelated soft matter via multimaterial multinozzle 3D printing, Nature. 575 (2019) 330–335, https://doi.org/10.1038/s41586-019-1736-8.

[10] C. Coulais, E. Teomy, K. De Reus, Y. Shokef, M. Van Hecke, Combinatorial design of textured mechanical metamaterials, Nature. 535 (2016) 529–532, https://doi.org/10.1038/nature18960.

[11] J.O. Hardin, T.J. Ober, A.D. Valentine, J.A. Lewis, Microfluidic printheads for multimaterial 3D printing of viscoelastic inks, Adv. Mater. 27 (2015) 3279–3284, https://doi.org/10.1002/adma.201500222.

[12] X. Chen, H. Zhou, Y. Li, Effective design space exploration of gradient nanostructured materials using active learning based surrogate models, Mater. Des. 183 (2019) 108085, https://doi.org/10.1016/j.matdes.2019.108085.

[13] C.T. Chen, D.C. Chrzan, G.X. Gu, Nano-topology optimization for materials design with atom-by-atom control, Nat. Commun. 11 (2020) 1–9, https://doi.org/10.1038/s41467-020-17570-1.

[14] M. Osanov, J.K. Guest, Topology optimization for architected materials design, Annu. Rev. Mater. Res. 46 (2016) 211–233, https://doi.org/10.1146/annurev-matsci-070115-031826.

[15] Z. Yang, Y.C. Yabansu, D. Jha, W.-K. Liao, A.N. Choudhary, S.R. Kalidindi, A. Agrawal, Establishing structure-property localization linkages for elastic deformation of three-dimensional high contrast composites using deep learning approaches, Acta Mater. 166 (2019) 335–345.

[16] C. Yang, Y. Kim, S. Ryu, G.X. Gu, Prediction of composite microstructure stress-strain curves using convolutional neural networks, Mater. Des. 189 (2020) 108509, https://doi.org/10.1016/j.matdes.2020.108509.

[17] Z. Yang, C.H. Yu, M.J. Buehler, Deep learning model to predict complex stress and strain fields in hierarchical composites, Sci. Adv. 7 (2021), https://doi.org/10.1126/SCIADV.ABD7416.

[18] M. Raj, S. Thakre, R.K. Annabattula, A.K. Kanjarla, Estimation of local strain fields in two-phase elastic composite materials using UNet-based deep learning, Integr. Mater. Manuf. Innov. 10 (2021) 444–460, https://doi.org/10.1007/s40192-021-00227-2.

[19] D. Montes de Oca Zapiain, E. Popova, S.R. Kalidindi, Prediction of microscale plastic strain rate fields in two-phase composites subjected to an arbitrary macroscale strain rate using the materials knowledge system framework, Acta Mater. 141 (2017) 230–240.

[20] M.I. Latypov, L.S. Toth, S.R. Kalidindi, Materials knowledge system for nonlinear composites, Comput. Methods Appl. Mech. Eng. 346 (2019) 180–196, https://doi.org/10.1016/j.cma.2018.11.034.

[21] Y.C. Yabansu, A. Iskakov, A. Kapustina, S. Rajagopalan, S.R. Kalidindi, Application of Gaussian process regression models for capturing the evolution of microstructure statistics in aging of nickel-based superalloys, Acta Mater. 178 (2019) 45–58, https://doi.org/10.1016/j.actamat.2019.07.048.

[22] E. Samaniego, C. Anitescu, S. Goswami, V.M. Nguyen-Thanh, H. Guo, K. Hamdia, X. Zhuang, T. Rabczuk, An energy approach to the solution of partial differential equations in computational mechanics via machine learning: Concepts, implementation and applications, Comput. Methods Appl. Mech. Eng. 362 (2020) 112790.

[23] X. Zhuang, H. Guo, N. Alajlan, H. Zhu, T. Rabczuk, Deep autoencoder based energy method for the bending, vibration, and buckling analysis of Kirchhoff plates with transfer learning, Eur. J. Mech. A/Solids. 87 (2021) 104225, https://doi.org/10.1016/j.euromechsol.2021.104225.

[24] Y. Kim, Y. Kim, C. Yang, K. Park, G.X. Gu, S. Ryu, Deep learning framework for material design space exploration using active transfer learning and data augmentation, NPJ Comput. Mater. 7 (1) (2021), https://doi.org/10.1038/s41524-021-00609-2.

[25] W. Demeke, Y. Kim, J. Jung, J. Chung, B. Ryu, S. Ryu, Neural network-assisted optimization of segmented thermoelectric power generators using active learning based on a genetic optimization algorithm, Energy Rep. 8 (2022) 6633–6644, https://doi.org/10.1016/j.egyr.2022.04.065.

[26] S. Ryu, S. Lee, J. Jung, J. Lee, Y. Kim, Micromechanics-based homogenization of the effective physical properties of composites with an anisotropic matrix and interfacial imperfections, Front. Mater. 6 (2019) 1–17, https://doi.org/10.3389/fmats.2019.00021.

[27] J.R. Mianroodi, N.H. Siboni, D. Raabe, Teaching solid mechanics to artificial intelligence—a fast solver for heterogeneous materials, NPJ Comput. Mater. 7 (2021) 1–10, https://doi.org/10.1038/s41524-021-00571-z.

[28] X. Ding, X. Zhang, Y. Zhou, J. Han, G. Ding, J. Sun, Scaling Up Your Kernels to 31x31, Revisiting Large Kernel Design in CNNs (2022). http://arxiv.org/abs/2203.06717.

[29] M. Li, X. Li, W. Sun, X. Wang, S. Wang, Efficient convolutional neural network with multi-kernel enhancement features for real-time facial expression recognition, J. Real-Time Image Process. 18 (2021) 2111–2122, https://doi.org/10.1007/s11554-021-01088-w.

[30] P.G. Young, T.B.H. Beresford-West, S.R.L. Coward, B. Notarberardino, B. Walker, A. Abdul-Aziz, An efficient approach to converting three-dimensional image data into highly accurate computational models, Philos. Trans. R. Soc. A Math. Phys. Eng. Sci. 366 (2008) 3155–3173, https://doi.org/10.1098/rsta.2008.0090.

[31] F.L. Palombini, E.L. Lautert, J.E.d.A. Mariath, B.F. de Oliveira, Combining numerical models and discretizing methods in the analysis of bamboo parenchyma using finite element analysis based on X-ray microtomography, Wood Sci. Technol. 54 (1) (2020) 161–186.

[32] R. Cimrman, V. Lukeš, E. Rohan, Multiscale finite element calculations in python using sfepy, ArXiv. 45 (4) (2019) 1897–1921.

[33] A. Taliercio, Generalized plane strain finite element model for the analysis of elastoplastic composites, Int. J. Solids Struct. 42 (2005) 2361–2379, https://doi.org/10.1016/j.ijsolstr.2004.09.030.

[34] Y. Zhang, Z. Xia, F. Ellyin, Two-scale analysis of a filament-wound cylindrical structure and application of periodic boundary conditions, Int. J. Solids Struct. 45 (2008) 5322–5336, https://doi.org/10.1016/j.ijsolstr.2008.05.026.
[35] S. Santurkar, D. Tsipras, A. Ilyas, A. Madry, How does batch normalization help optimization?, Adv Neural Inf. Process. Syst. (2018) 2483–2493.
[36] F. Ren, W. Liu, G. Wu, Feature reuse residual networks for insect pest recognition, IEEE Access. 7 (2019) 122758–122768, https://doi.org/10.1109/ACCESS.2019.2938194.
[37] S. Kriman, S. Beliaev, B. Ginsburg, J. Huang, O. Kuchaiev, V. Lavrukhin, R. Leary, J. Li, Y. Zhang, Quartznet: deep automatic speech recognition with 1D time-channel separable convolutions, in: ICASSP IEEE Int. Conf. Acoust. Speech Signal Process. - Proc. 2020-May, 2020, pp. 6124–6128, https://doi.org/10.1109/ICASSP40776.2020.9053889.
[38] D.P. Kingma, J.L. Ba, Adam: a method for stochastic optimization, in: 3rd Int. Conf. Learn. Represent ICLR 2015 Conf. Track Proc., 2015, pp. 1–15.
[39] A.S. Rao, T. Nguyen, M. Palaniswami, T. Ngo, Vision-based automated crack detection using convolutional neural networks for condition assessment of infrastructure, Struct. Heal. Monit. 20 (2021) 2124–2142, https://doi.org/10.1177/1475921720965445.
[40] S. Yang, C. Zhao, J. Ren, K. Zheng, Z. Shao, S. Ling, Acquiring structural and mechanical information of a fibrous network through deep learning, Nanoscale. 14 (2022) 5044–5053, https://doi.org/10.1039/d2nr00372d.
[41] T.R. Hayes, J.M. Henderson, Deep saliency models learn low-, mid-, and high-level features to predict scene attention, Sci. Rep. 11 (2021) 1–13, https://doi.org/10.1038/s41598-021-97879-z.
[42] S. Ghosal, D. Blystone, A.K. Singh, B. Ganapathysubramanian, A. Singh, S. Sarkar, An explainable deep machine vision framework for plant stress phenotyping, Proc. Natl. Acad. Sci. U.S.A. 115 (2018) 4613–4618, https://doi.org/10.1073/pnas.1716999115.
[43] B.S.S. Pokuri, S. Ghosal, A. Kokate, S. Sarkar, B. Ganapathysubramanian, Interpretable deep learning for guided microstructure-property explorations in photovoltaics, NPJ Comput. Mater. 5 (2019) 1–11, https://doi.org/10.1038/s41524-019-0231-y.